Analyst

A Micro Passive Preconcentrator for Micro Gas Chromatography

Journal:	*Analyst*
Manuscript ID	AN-ART-07-2020-001485.R1
Article Type:	Paper
Date Submitted by the Author:	10-Sep-2020
Complete List of Authors:	Zhan, Changhua; University of Michigan, Akbar, Muhammad; University of Michigan Hower, Robert; University of Michigan, Environmental Health Services Nuñovero, Nicolas; University of Michigan, Potkay, Joseph; VA Ann Arbor Healthcare System, Advanced Platform Technology Center Zellers, E; University of Michigan, Dept. of Environmental Health Sciences

A Micro Passive Preconcentrator for Micro Gas Chromatography†

Changhua Zhan,[ad] Muhammad Akbar,[ad] Robert Hower,[ad] Nicolas Nuñovero,[ad] Joseph A. Potkay[bd]* and Edward T. Zellers[acd]*

[a]*Department of Environental Health Sciences, University of Michigan, Ann Arbor, MI, USA*
[b]*Department of Surgery, University of Michigan, Ann Arbor, MI, USA*
[c]*Department of Chemistry, University of Michigan, Ann Arbor, MI, USA*
[d]*Center for Wireless Integrated MicroSensing & Systems (WIMS2), University of Michigan, Ann Arbor, MI, USA.*

† Electronic Supplementary Information (ESI) available: See DOI: xx.xxx/yyyyyyyyyy

We describe a microfabricated passive preconcentrator (μPP) intended for integration into gas chromatographic microsystems (μGC) for analyzing volatile/semi-volatile organic compounds (S/VOC). Devices (8 × 8 mm) were made from a silicon-on-insulator top layer and a glass bottom layer. The top layer has 237 apertures (47 × 47 μm) distributed around the periphery of a circular region (5.2-mm o.d.) through which ambient vapors diffuse at predictable rates. Two internal annular cavities offset from the apertures are packed with ~800 μg each of commercial carbon adsorbents. Thin-film heaters thermally desorb captured vapors, which are drawn by a pump through a central exit port to a micro injector for analysis with a bench scale GC. The 15 test compounds spanned a vapor pressure range of 0.033 to 1.1 kPa. Effective (diffusional) μPP sampling rates ranged from 0.16 to 0.78 mL/min for short-duration exposures to ~mg/m^3 vapor concentrations. Observed and modeled sampling rates generally agreed within 15%. Sampling rates for two representative compounds declined by ≤ 30% between 0.25 and 24 hr of continuous exposure. For one of these, the sampling rate declined by only 8% over a ~2,300-fold concentration range (0.25-hr samples). Desorption (transfer) efficiencies were > 95% for most compounds (250-275 °C, 60 sec, 5 mL/min). Sampling rates for mixtures matched those for the individual compounds. Dissipating no energy while sampling, additional advantages of this novel device include short- or long-term sampling, high capacity and transfer efficiency for a diverse set of S/VOCs, low transfer flow rate, and a robust fabrication process.

Introduction

Gas chromatographic instrumentation employing Si-microfabricated analytical components (μGC) show great promise for near-real-time measurements of the composition of vapor-phase mixtures of volatile and semi-volatile organic compounds (S/VOCs) at low power and in small packages. Such technology would facilitate worker exposure measurements, distributed networks for monitoring industrial processes and air pollution, point-of-care health status assessments, and numerous applications of interest to the intelligence community and the military. Reports of μGCs containing microfabricated devices for sample capture, injection, separation, and/or detection have appeared over the

last decade or so,[1-12] and a resurgence of commercialization efforts related to such technologies is also apparent.[13-16]

Since preconcentration is necessary to detect the low concentrations of target vapors demanded in many applications, μGCs often incorporate (μ)preconcentrators containing one or more adsorbent material and an integrated heater.[1-4,7-11,12] Typically, vapors in an air sample, drawn through the device with a small pump, are retained on the adsorbent(s) by physisorption and subsequently thermally desorbed into a smaller volume of carrier gas. This increases vapor concentrations and narrows the injection band width prior to downstream separation and detection.[17-22]

Power efficiency is often integral to device design and operation. In most reported μGC prototypes, commercial diaphragm mini-pumps are used to capture air samples.[1,2,4-11] A typical average power consumed by such pumps is ~300 mW. For short-duration sampling, the energy consumed by the pump (i.e., 18 J/min) is a small fraction of the total energy per analysis (e.g., 2.2 kJ per 6-min analytical cycle for the belt-mounted μGC described in ref. 11). But, for sampling periods > 0.5 hr, pumping starts to dominate the energy budget, and for battery-powered systems this may preclude applications requiring longer sampling times.

In a previous article, our group described a so-called microfabricated passive preconcentrator-injector (μPPI) that collects vapors at known rates by molecular diffusion.[23] Packed with a graphitized carbon adsorbent, Carbopack X (C-X), the μPPI exhibited an effective diffusional sampling rate for toluene of ~9 mL/min, a high thermal desorption efficiency, and stable long-term operation.

Yet, the μPPI had several drawbacks. First, the sampling rate began to decline after only 30 min of exposure to toluene at 1 ppm because of the limited adsorption capacity of the single adsorbent used. In addition, an extremely high desorption flow rate of 50 mL/min was required to avoid losing part of the vapor sample to back diffusion through the aperture grid during thermal desorption. This desorption flow rate is much too high for μGC separations. Furthermore, it was not possible to generate a narrow injection band due to its relatively large internal volume, non-uniform flow, and limited heating rate. Lastly, the fabrication process was cumbersome and device yields were low. Subsequent testing of the μPPI with a small set of VOCs confirmed its low capacity, broad injections, and low-quality GC separations.[24]

The research described here is part of a larger project concerned with developing a so-called microfabricated collector-injector (μCOIN) that could serve as a front-end of any μGC for S/VOC mixture analysis. As conceived, the μCOIN would consist of two integrated devices, a *micro passive preconcentrator* (μPP) and a *micro progressively heated injector* (μPHI). The μPP would passively collect vapors from the atmosphere and trap them onto one of two judiciously chosen internal adsorbents. It then would desorb them thermally and pass them as a broad, semi-concentrated bolus to the μPHI device in a 'few-mL' transfer volume under active flow provided by a downstream mini-pump. The μPHI device, in turn, would capture the vapors in the transferred sample and then inject the entire vapor mixture as a sharply focused (i.e., 'few μL') band to a downstream separation (micro)column at a low flow rate, thereby enabling efficient chromatographic resolution of mixture components and detection by a downstream detector. Preliminary reports on the μPP and μPHI have been published in two conference proceedings papers.[25,26] Here we report only on the μPP.

The goals of this effort were defined in terms of several performance criteria applicable to a μCOIN-μGC system associated with monitoring for markers of illicit activities (e.g., terrorist threats) and environmental pollutants.[27] Prominent among these were small size, minimum and maximum sampling periods of 0.5 and 24 hr, respectively, detectable concentrations as low as 0.05 mg/m^3, and (low-power) deployment for several months of unattended operation on battery power.

Here we present the design and characterization of the first-generation μPP using a structurally diverse set of target compounds tested individually and in simple mixtures over a range of time periods and concentrations. A semi-empirical model of the physicochemical processes governing vapor transport, uptake, and desorption is introduced. Using a benchscale GC with flame-ionization detector (FID) for quantitative analysis, an emphasis is placed on documenting and rationalizing observed sampling rates, capacities, and desorption (transfer) efficiencies to inform next-generation designs.

Background

The effective diffusional sampling rate of a passive sampling device, S_e (cm^3/s), by analogy with an actively pumped sampler flow rate, is the volume of contaminated air drawn into the device per unit time. From Fick's first law:[28-30] $S_e = DA/L = m/(C_a t)$, where D is the vapor diffusion coefficient in air (cm^2/s), A is the cross-sectional area (cm^2) and L is the length (cm) of the diffusion path within the device, C_a is the air concentration of the ambient vapor (μg/cm^3), and m is the mass of vapor captured (μg) over time, t (s). It is assumed that the concentration of vapor at the surface of the adsorbent placed at the end of the diffusion path is zero, such that there is a linear concentration gradient from the ambient to the adsorbent. Since m is proportional to C_a, S_e is independent of C_a. With proper design,[29] Fickian diffusion governs mass transfer, and for a constant A/L ratio the device can be scaled down in size with no change in S_e.

Among the factors affecting device performance are the diffusion coefficients and adsorption capacities for the target vapors during sampling, and the desorption rates, efficiencies, and band widths during transfer. All of these factors depend on the concentrations, volatilities, and structures of the S/VOC(s); the mass, functionality, porosity, and specific surface area of the adsorbent; and the flow rate of the air or carrier gas being drawn through the device during sampling or desorption/injection, respectively. Desorption is also affected by the heating rate and maximum temperature, T_{max}.

The amount of vapor retained on the surface of a porous solid adsorbent at equilibrium determines the adsorption capacity, W_e, which is the ratio of the mass of adsorbed vapor to the mass of adsorbent at a given air concentration.[30,31] At concentrations where coverage is << a monolayer and an excess of adsorption sites is available, vapors with sufficient affinity will be well-retained on the adsorbent surface; the vapor concentration just above the adsorbent surface should be negligible. Although W_e varies directly with C_a, such that capacity increases with concentration, the dependence is invariably a steadily decreasing function of C_a, consistent with a classical Type II (e.g., Langmuir) isotherm.[32,33] With further increases in C_a, W_e will eventually reach a maximum, corresponding to monolayer coverage (occupancy) of adsorption sites on the solid.

Even at sub-monolayer coverage, weakly adsorbed vapors may partially desorb spontaneously. In the context of the (passive) μPP, this could result in a reduction in the concentration gradient, redistribution across the adsorbent bed(s), or off-gassing following

an initial exposure, any of which would cause a decrease in S_e. In practice, this might occur as a function of time for a fixed vapor concentration, as a function concentration for a fixed sampling time, or as a function of competition for exposure to a mixture of vapors. Although some reduction in S_e may be tolerable, at some point quantitative analysis would be undermined.

Thermal desorption and transfer of the captured vapors downstream (e.g., to the micro-focuser of the μCOIN) requires active suction flow through the device. During this step, the temperature must be high enough to overcome the heat of adsorption for the vapor(s), and the transfer flow rate must be sufficient to overcome the back-diffusion caused by the heating process to avoid loss of the vapors back through the inlet aperture.

Experimental

Materials

Test compounds and solvents were purchased from Acros/Fisher (Pittsburgh, PA) or Sigma–Aldrich/Fluka (Milwaulkee, WI) in > 90% purity (most >99%) and used as received. Carbopack C-X (240 m^2/g) and Carbopack B (C-B, 100 m^2/g) were obtained from Supelco (Bellefonte, PA) and were manually sieved to isolate granules with nominal diameters ranging from 224-250 μm. Silicon-on-insulator (SOI) wafers (4" diam.) with a 180-μm (Si) device layer, a 1.5-μm buried oxide layer, and a 380-μm (Si) handle layer were obtained from University Wafer, Boston, MA, as were borofloat glass wafers (4" diam., 200 μm thick).

μPP fabrication

Deep reactive ion etching (DRIE) of the top silicon-on-insulator (SOI) substrate was used to form the critical features, including the aperture grid, adsorbent-retention pillars, adsorbent loading ports, and the fluidic transfer channel. Thin metal resistive heater films and co-located resistive temperature detectors (RTD) for thermal desorption of captured vapors were deposited on the bottom glass substrate. Section S1 of the Electronic Supporting Information, ESI (†), describes the details of the fabrication procedure, along with supporting images and diagrams (Figures S1-S3†).

To perform analyses by GC-FID it was necessary for most tests to use a focusing device that could accept desorbed samples transferred from the μPP under suction flow provided by a mini-pump and inject them directly into the GC column under a positive pressure of carrier gas. Since the companion μPHI development effort lagged behind that of the μPP, as an interim measure we used our previously developed μpreconcentrator-focuser (μPCF) which has been extensively characterized and used reliably in prototype μGC instruments.[11,20] Figure S4† presents a photograph and brief description of the μPCF device. Details of the fabrication of the μPCF can be found elsewhere.[20]

Device filling, sealing, mounting

A ~25-cm segment of deactivated fused silica capillary (250 μm i.d.) was inserted into the tapered outlet channel of the μPP and sealed with Duraseal (Cotronics Corp., New York, NY). The inner and outer cavities were loaded sequentially with ~780 μg of C-X and ~830 μg of C-B, respectively, by applying gentle suction to the outlet capillary and drawing the

granules of each material in through the fill ports. The device was weighed (±10 μg) before and after each adsorbent was loaded, and the extent of filling was also monitored visually. After filling and weighing, the corresponding fill port(s) was sealed with Duraseal and allowed to cure overnight.

The μPP was anchored with epoxy (Hysol 1C, Henkel Corporation, Rocky Hill, CT) onto a custom printed circuit board (PCB) which had a square hole beneath the device for thermal isolation from the PCB substrate. The capillary was also anchored with Hysol to the PCB to relieve stress on the junction with the device. The PCB surface was coated with a thin layer of Au by the supplier to minimize adsorption of vapors during subsequent testing in the exposure chamber. The bonding pads on the μPP device were wire-bonded to pads on the PCB. Note that two devices were used over the course of the study. The sampling rates were checked and found to be identical for the four test vapors used to compare performance.

The μPCF was filled, sealed, mounted and wirebonded on a separate custom PCB in a manner similar to that for the μPP using the same adsorbent materials.[11] The μPCF used three segments of ~15-cm deactivated fused silica capillary (250 μm i.d.,) to connect to the μPP and the mini-pump during sample transfer, and to a tank of compressed He carrier gas and the GC inlet during injection; a 6-port valve allowed loading in one direction and then desorption/injection with backflushing. The voltage outputs from the RTDs of the μPP and μPCF were calibrated in the GC oven.

Test system and exposure chamber

The system used to generate and confirm test atmosphere concentrations, expose the μPP, and collect and analyze the samples transferred from the μPP is described in Section S2† and shown schematically in Figure S5†. Scrubbed house air was passed through mass flow controllers to generate the dilution flow. A portion of this stream was diverted and passed through a fritted bubbler containing the liquid test compound to generate a quasi-saturated stream of vapor and that was directed back into the dilution air stream and through a downstream mixing chamber. A three-way solenoid valve placed just upstream of the stainless steel chamber housing the μPP (Figure S6†) had paths leading to the chamber or the hood. An upstream tee allowed switching to a N_2 purge. The flow through the chamber was controlled to ~1 L/min.

A portion of the downstream atmosphere was collected by a sampling loop and injected into the GC-FID by a positive flow of N_2 for concentration confirmation. All downstream stainless-steel tubing or deactivated fused-silica capillary and connectors were wrapped with coil heaters, heater-embedded polymer pads (Omega Engineering, Norwalk, CT) or custom coil reinforced tubing (MicroLumen, Oldsmar, FL). Thermocouples were installed at several points in the flow path. Lines were heated to 70 °C for tests with compounds where adsorption to surfaces was of concern.

Two 6-port valves (VICI-Valco, Houston, TX) in an ovenized enclosure were used to direct flow as needed. Analyses of test atmosphere concentrations and μPP samples transferred to (and injected from) the μPCF were performed with a bench scale GC-FID (6890, Agilent Technologies, Palo Alto, CA) calibrated with liquid solutions of the S/VOCs.

Testing procedures

In a typical sampling test, the exposure chamber was purged with N_2 (or clean air) and a background sample was taken and injected into the GC via sampling loop to ensure no residual vapor was present. Then, a blank was transferred from the heated μPP to the μPCF and analyzed. This procedure was repeated as needed to obtain a clean blank chromatogram. Leak testing was conducted periodically with a helium leak detector and any leaks were sealed prior to testing.

Every few minutes, a portion of the test atmosphere collected by sampling loop was injected into the GC-FID for concentration confirmation. Once the exposure period was over, the chamber was purged with N_2 for at least 4 min to remove any vapor, and the mini-pump was activated to draw flow through the μPP transfer line at 5 mL/min through the μPCF. The μPP heaters were then activated and the μPP heated to 250 °C (or higher, see below) for 60 sec. Then the pump was turned off and the μPP allowed to cool down without flow passing through it. During sampling, the transfer line emanating from the μPP was blocked using a termination in place of the mini-pump connection to the 6-port valve to avoid any inadvertent advective flow through the device.

Following the sample transfer, the 2nd 6-port valve was switched to pass carrier gas through the μPCF while it was heated to 250 °C for 60 sec to inject the transferred sample with backflushing into the GC inlet. For most tests, a series of three transfer/desorption cycles was performed to ensure complete desorption of the collected sample and to enable calculation of the sampling rate and desorption efficiency.

Sampling rate calculations were based on the total mass detected from all transfers and injections. Assuming all of the collected sample was released/transferred ultimately, the desorption efficiency (*DE*) value was calculated as the ratio of the first injected mass over the total injected mass. For one series of tests with o-xylene a mini-photoionization detector (PID, NovaPID, Nanova, Columbia, MO) was installed in line between the pump and μPP to examine the transferred peak width at 3 and 5 mL/min.

Thermogravimetric analysis (TGA)

A thermogravimetric analyzer (TGA, Pyris 1, Perkin Elmer, Waltham, MA) was used to measure vapor uptake, retention, and thermal desorption by C-X or C-B using samples loaded into the weighing pan of the TGA, suspended from the balance, and preconditioned at 250 °C under N_2 for >30 min. Details of the set-up and procedures are in Section S3†.

Heater control, parameter adjustment, data acquisition, data analysis

A laptop computer running custom LabVIEW (Ver. 14.0, National Instruments, Austin, TX) programs was used to control the μPP and μPCF heaters. Operating parameter settings and control functions were entered through a graphical user interface (GUI). Independent proportional-integral-derivative (PID) feedback loops were designed to control heating rates and temperatures via solid-state relays and pulse-width modulation (PWM) of the generated signals. For each device, a separate 16-bit DAQ card (NI USB-6216 OEM and NI USB-6212, National Instruments) was used to record the PWM voltage applied to each heater at a sampling rate of 250 Hz.

The temperature profiles of the μPP heaters were characterized with the loaded μPP. Figure S7† shows a set of profiles for one heating sequence from the RTDs located adjacent to the heaters in the inner and outer adsorbent-bed cavities, as well as on the chip outside of the device. The heating rate was intentionally set at a modest value of ~ 50 °C/sec to

reduce the likelihood of losses due to back diffusion through the aperture grid. The cavity heaters tracked each other closely and reached their T_{max} of 250 °C within ~6 sec. The chip temperature rose to a lower T_{max} of 210 °C because of conduction through the substrate (note: the chip heater was not used). This heating profile was highly reproducible and the device was heated hundreds of times without failure. Subsequent experiments used a T_{max} of 275 °C to improve the *DE* of DEMP.

For heating the μPCF, an initial fast ramp of 400 °C/sec was used to heat from ambient temperature to 100 °C, followed by a PWM ramp of 150 °C/sec to 250 °C, which was maintained for 60 s to ensure that even the least volatile test compounds would be completely desorbed.[4,20,39] Injected samples were passed via a capillary to the FID or to the head of a capillary column for separation (where necessary) and then to the FID. For compounds with vapor pressures, p_v, < 1 kPa, the transfer line was heated to 70 °C.

The 6-port valves, interconnect heaters, and 3-way solenoid valve upstream of the chamber were actuated (switched on and off) manually. Chemstation software (Agilent) controlled GC flow rates, temperatures, and oven temperature programming. Raw chromatogram traces were stored as text files and analyzed using OriginPro (Ver. 9.1, OriginLab, Northampton, MA) for peak integrations. Additional analyses and modeling were performed with Excel (Office 365, Microsoft, Redmond, WA).

Results and discussion

Design and operation

Device description. Figures 1a-d show top- and side-view conceptual diagrams of the μPP device during diffusional sampling (Figure 1a, b) and pumped/heated desorption/transfer (Figure 1c,d). Figure 1e shows the CAD layout drawing specifying the critical device features. Each device was made from a top silicon-on-insulator substrate and a bottom glass substrate. Each device chip measures ~ 8 mm × 8 mm (Figure 1e). Figure 1f is a photomicrograph of the μPP viewed from the glass underside. The inset is an IR image of a section of the periphery showing the apertures and the pillar locations. SEMs of the pillars and apertures are presented in Figure 1g and h, respectively. Figure 1i shows the μPP, with interconnecting capillary, mounted and wire-bonded to its PCB.

The μPP contains an array of apertures at the periphery of its circular outer boundary through which vapors diffuse to the interior of the device. Although designed to have dimensions of 50 × 50 μm, due to a masking error, the actual dimensions were 47 × 47 μm. Just within this ring of apertures is the first annular adsorbent cavity, the boundaries of which are defined by cylindrical pillars (~180 μm o.d., spaced by 130 μm) that retain the adsorbent. This cavity had a radial length of 610 μm and was loaded with the lower-surface-area C-B. The two outer-bed fill ports are located at opposite sides of the annular cavity and comprise straight channels with tapered inlets formed in the top substrate. Concentrically internal to the C-B cavity is the inner cavity, the inner boundary of which is defined by a third ring of pillars. This cavity had a radial length of 462 μm and was filled with C-X. The single fill port for this cavity is located at 90 ° from the C-B fill ports. At the center of the device is an empty cavity (2 mm diameter) from which the fluidic port emanates and through which air is drawn during thermal desorption and transfer of preconcentrated vapor samples.

Lining the floor of each cavity are Ti/Pt thin-film resistive heaters and RTDs, the origins and terminations of which are located at one of the four wire-bonding areas at the corners of the chip.

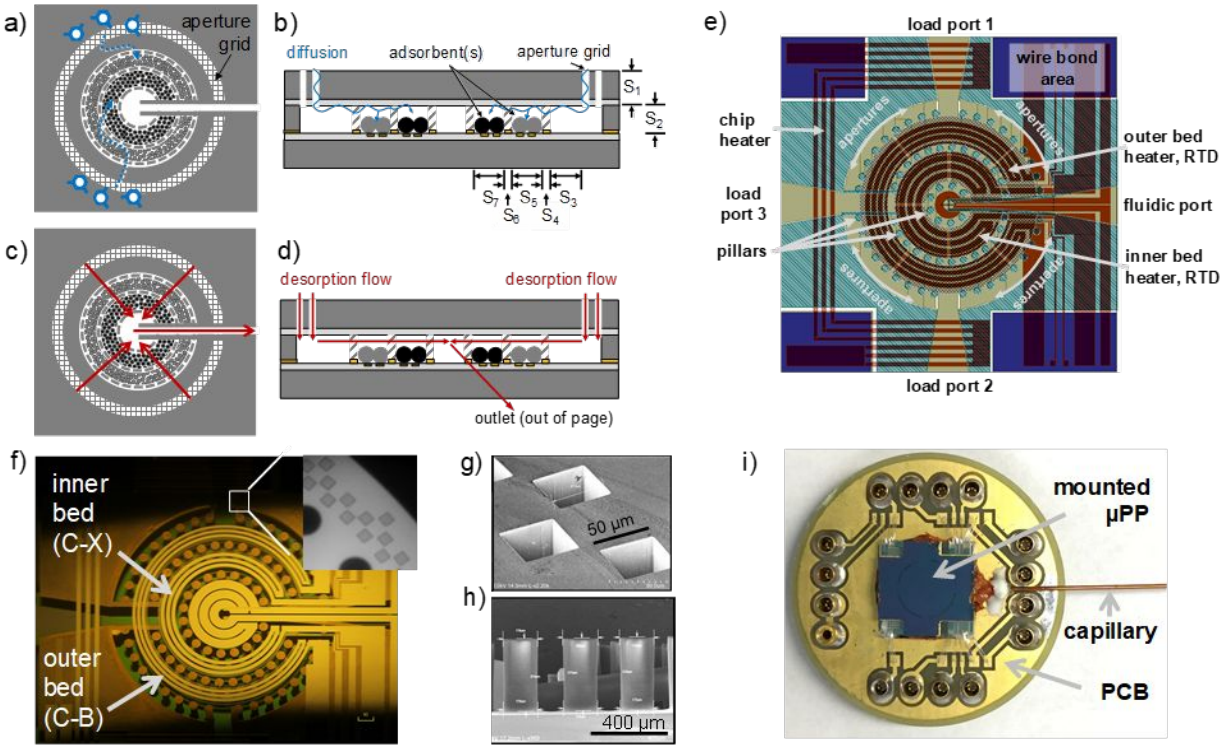

Figure 1 (a)-(d) Top and side view conceptual drawings of the µPP illustrating key features of the design and operation; A_i and L_i are the cross-sectional area and length of the formalized diffusion path segments (i = 1, 2, 3) used for modeling; (e) CAD layout for the µPP with key components labeled; (f) bottom view microscopic image of completed µPP -- inset is an IR image of a section of the periphery showing the apertures and bonding locations of the pillars; (g) SEM of a section of apertures; (h) SEM (side view) of adsorbent retention pillars; (i) PCB-mounted µPP chip (8 mm × 8 mm) with interconnecting capillary.

Design rationale. To rationalize the µPP design and operation, several factors were considered related to both the sampling function and desorption/transfer function, which were dependent on the S/VOCs. For this initial study we limited the S/VOCs we pursued for quantitative sampling and transfer to those falling within the p_v range of 0.03 to 1.11 kPa to avoid problems with capture efficiency for more volatile compounds and desorption efficiency for less volatile compounds. Table 1 lists the compounds tested and their relevant physical properties.

Accordingly, we selected the graphitized carbons C-X (240 m^2/g) and C-B (100 m^2/g) as adsorbent materials based on our previous studies showing that they exhibited the right balance of capacity and desorption efficiency for compounds in this p_v range.[10,20] The C-B in the outer cavity, which is "upstream" with respect to the direction of diffusion during

sampling, combines high capacity with high desorption efficiency for less volatile compounds. The inner, "downstream" cavity contains the higher-surface-area C-X which is better suited for trapping/desorbing more volatile compounds.[4,40] Both C-X and C-B are hydrophobic and stable in air at high temperatures, and have been used successfully in a number of μGC systems on which we have reported.[4,10,11,20,40] We designed the cavities to hold roughly 800 μg each of C-X and C-B, assuming a packing density of ~0.4 g/cm^3 .[23,41]

The number and size of the apertures were selected to give a nominal initial sampling rate, S_e, of ~0.66 mL/min for our primary model compound, m-xylene (see below). This value of S_e would allow collection of ~ 1 ng in 30 min at 0.05 mg/m^3, which were the specified sampling time and concentration. A minimum mass of 0.5 ng was chosen as likely to be detectable by a downstream detector, such as a PID,[42] MS[43] or a sensor array.[11] Furthermore, this would result in the collection of <50 ng in 24 hr at the same minimum concentration, which is well below the expected adsorption capacity for m-xylene and, thus, allows for the presence of other co-adsorbed compounds (see below for discussion of capacity as a function of concentration).

Table 1 Results of short-term performance tests of the μPP with 15 individual compounds.

Compound[a]	p_v (kPa)[b]	D (cm^2/s)[c]	C_o (mg/m^3)	S_e (mL/min)			0.5-hr uptake (ng)[g]
				Model[e]	Exper.	Ratio	
m-xylene	1.1	0.068	44	0.61	0.65	1.1	0.98
o-xylene	0.89	0.072	40	0.65	0.66	1.0	0.99
isoamyl acetate	0.75	0.068	15	0.61	0.57	0.93	0.86
cyclohexanone	0.58	0.078	23	0.70	0.64	0.91	0.96
CEES	0.45	0.074	36	0.67	0.67	1.0	1.0
DMMP	0.13	0.050	49	0.45	0.44	0.98	0.66
cyclohexanol	0.088	0.076	42	0.69	0.62	0.90	0.93
PFTBA	0.074	0.033	47	0.30	0.33	1.1	0.50
NBZ	0.033	0.079	28	0.71	0.78	1.1	1.2
DIMP	0.037	0.028	17	0.25	0.21	0.84	0.32
DEMP	0.039	0.036	42	0.32	0.26	0.81	0.39
NMP	0.047	0.087	48	0.79	0.34[d]	0.43	0.51
DMSO	0.080	0.098	52	0.88	0.16[d]	0.18	0.29
1-butanol	0.93	0.087	198	0.49[f]	0.31	0.63	0.47
DMF	0.52	0.10	110	0.56[f]	0.41	0.73	0.62

[a] acronyms are defined as follows: CEES, chloroethylethyl sulfide; DMMP, dimethylmethyl-phosphonate; PFTBA, perfluorotributyl amine; NBZ, nitrobenzene; DIMP, diisopropylmethyl-phosphonate; DEMP, dimethylmethylphosphonate; NMP, N-methyl-2-pyrrolidione; DMSO, dimethylsulfoxide;,DMF, N,N-dimethylformamide; [b] at 25 °C from ref. 34; [c] at 25 °C from refs. 35-38 but for DEMP and DIMP please refer to Section S8 of the ESI; [d] thermal decomposition suspected – see text; [e] all values are initial ("time-zero") S_e values assuming no penetration into the C-B bed except for n-butanol and DMF; [f] model was run assuming no trapping in the C-B bed; [g] uptake mass calculated for a 0.5-hr exposure to 0.05 mg/m^3 using the experimental S_e values in this table.

The μPP was designed to address the major shortcomings of the predecessor μPPI device. The radial μPP topology with the grid of sampling apertures at the periphery and two concentric adsorbent bed regions (C-B and C-X) offset inwardly (Figure 1) was

adopted for several reasons. First, as mentioned above, during sampling the vapors would pass over the lower surface area C-B bed and then over the higher surface area C-X bed to expand the range of vapors efficiently sampled and transferred. Second, during desorption/transfer a more uniform distribution of swept flow would be generated laterally across the adsorbent beds to enhance capture efficiency and reduce the flow rate (see below) required to avoid losses from back diffusion. The offset of the aperture grid also addresses this factor. In the previous μPPI device the transfer flow was drawn predominantly from one side of the device through apertures located directly above the adsorbent bed. Another design change entailed reducing the sampling rate by reducing the number of apertures to allow longer term sampling prior to exceeding the adsorption capacity, while still being able to collect sufficient mass over shorter time periods to address this goal. The 2-fold increase in total adsorbent mass over the predecessor μPPI device would increase capacity and/or the maximum duration of sampling at a constant rate. In addition, the simpler fabrication process and structure promised higher yield and manufacturability.

Design modeling. For the μPP, the diffusion path can be formally divided into a series of seven segments (Figure 1b): 1) vertically through the grid of apertures, 2) vertically beneath the apertures, 3) laterally to the first set of pillars, 4) laterally through the spaces between pillars, 5) laterally through the outer adsorbent bed, 6) laterally through the second set of pillars, and 7) laterally through the inner adsorbent bed. Each of these can be considered to have separate values of A_i and L_i, and, therefore separate segmental sampling rates, S_i. At steady state, they can be summed in a manner analogous to a series of electrical conductances. Further imposing the constraints of mass balance and constant D yields the following expression:[23]

$$S_e = \frac{D}{\sum \frac{L_i}{A_i}} = \frac{1}{\sum \frac{1}{S_i}} \tag{1}$$

Modeling various design variations showed that the net value of S_e is initially limited by the aperture grid geometry (i.e., S_1 has the lowest value among the segments) but that S_5 (and S_7, if applicable) decreases with time as the adsorbent becomes saturated and vapors must diffuse further (laterally) toward the center of the μPP. Depending on the sampling period and the adsorption capacity for the vapor, this may lead to a reduction in S_e over time. The model developed to describe the impact of this factor on S_e is described below.

Power and energy efficiency were considered in the design but were deemed secondary to the fluidic factors. The average power and energy consumption values, estimated from the product of measured voltage and current waveforms, were 2 W and 120 J, respectively, assuming a 60-sec desorption/transfer period and a T_{max} of 300 °C. These low values would facilitate battery-powered operation of any portable system in which the μPP were incorporated.

Table 2 provides some of the modeled dimensions and expected operating features of the μPP. We used m-xylene as the basis for initial modeling. It has a p_v value of 1.1 kPa, and so was the most volatile member of our test set. DEMP (p_v = 0.039 kPa), was also modeled as one of the least volatile test compounds. Their diffusion coefficients, 0.068 and 0.036 cm^2/s, respectively (Table 1), differ by a factor of 1.9. The number and size of the apertures, along with the other diffusion path dimensions, gave modeled initial S_e values of 0.66 and 0.35 mL/min, respectively, permitting collection of ≥ 0.5 ng at 0.05 mg/m^3 in

30 min at 25 °C.

Table 2. µPP design and operating parameters.

Inner bed od/id[a]	2.92/2.00 mm
Outer bed od/id[a]	4.50/3.28 mm
Aperture #/ dimensions[b]	237/50×50 µm
L1/L2/L3/L4[c]	0.18/0.38/0.13/0.18 mm
L5/L6/L7[c]	0.61/0.18/0.46 mm
A1/A2/A3/A4[c]	0.59/2.4/3.7/1.5 mm^2
A5/A6/A7[c]	2.9/0.99/1.8 mm^2
Response time: m-xylene/DEMP[d]	32/60 ms
Expected S_e: m-xylene/DEMP	0.66/0.35 mL/min
Min. desorp. flow: m-xylene/DEMP	2.4/1.3 mL/min

[a] outer and inner diameters of the adsorbent bed cavities; [b] total number and lateral dimensions of grid of apertures (depth = 180 µm); [c] see Figure 1b (A5 and A7 are the avg. values across the adsorbent cavities assuming diffusion radially through the adsorbent beds); [d] time to reach steady state concentration at the start of the outer adsorbent cavity (i.e., the time to diffuse through segments S1-S4).

The required desorption flow rates (Table 2) were calculated in a manner similar to the sampling rates, assuming that D increases as $(T_2/T_1)^2$.[44] A temperature of 300 °C was assumed and the flow rate required to exceed that due to the 'reverse diffusion' of vapors driven off the adsorbent was 3.7× higher than that at ambient temperature (i.e., $[573/298]^2$): 2.4 mL/min for m-xylene and 1.3 mL/min for DEMP. To account for advective flow and to add a safety factor, we settled on a desorption flow rate of 5 mL/min, which is easily achieved with a diaphragm mini-pump due to the low pressure drop (< 0.23 kPa). This corresponds to a time to sweep the cavity of < 240 ms. In fact, the highest T_2 value we used was 275 °C. Normally, one would prefer to back flush from higher to lower surface area adsorbent during desorption to avoid band broadening, but this was not possible here and was also considered less critical because of the (ultimate) use of the companion µPHI (focuser/injector).

TGA mass uptake, off-gassing, and desorption efficiency

Section S5† presents the initial TGA results. Figure S8† shows the adsorption isotherm of m-xylene with C-X, which we could fit quite well to a Langmuir model; W_e increases with concentration but at a steadily decreasing rate. Values of W_e ranged from ~2,400 µg/g at 0.9 mg/m^3 to ~61,000 µg/g at 1,300 mg/m^3. Additional tests with C-X for other aromatic and aliphatic hydrocarbons (i.e., toluene, m-xylene, 1,2,4-trimethylbenzene and n-decane) at single concentrations of 4-6 mg/m^3 gave the expected linear dependence of W_e on p_v^{-1} as depicted in Figure S9†. The corresponding data for C-B were not collected.

In a companion study of C-B adsorption capacity in our group, conventional breakthrough tests were run with C-B or C-X packed in a metal tube continuously exposed to each of several individual test vapors at a single concentration.[45] Measured breakthrough masses, which should be proportional to W_e according to the Wheeler Model, gave the following relative values: 1.0, 0.33, 0.92, 1.3, and 2.0 for m-xylene, DMMP, DEMP, DIMP, and NBZ, respectively. For DMMP, the breakthrough mass with C-X was also

measured, and the ratio of breakthrough masses with C-X and C-B was 2.9 at the same concentration. Applying this ratio to the W_e values of m-xylene on C-X determined by TGA afforded estimates of W_e on C-B for m-xylene. Combining these with the ratios listed above yielded estimates of W_e on C-B for the other vapors. Similarly, tests of n-butanol with C-B showed immediate breakthrough, whereas with C-X the breakthrough mass was short but measurable, thereby permitting an estimate of W_e.[45] These estimates of W_e are presented in Table S1† and were used in the modeling discussed further below.

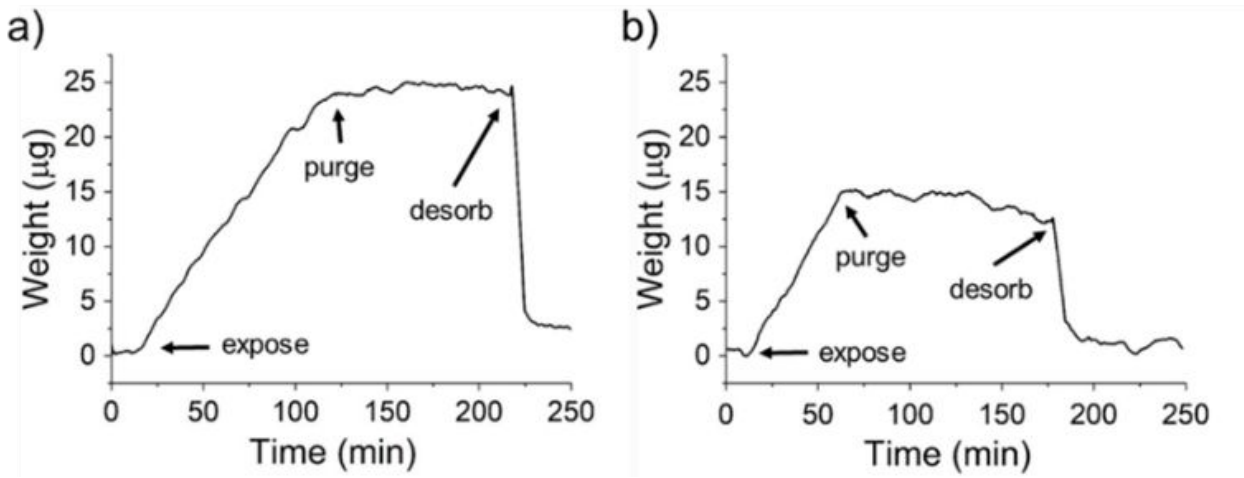

Figure 2 Results of TGA(exposure, purge, and desorption): (a) 2.9 mg C-X was exposed to 60 mg/m^3 of m-xylene for 100 min and N_2 for 120 min at ambient temperature, followed by thermal desorption at 250 °C; (b) 2.9 mg C-B was exposed to 78 mg/m^3 of m-xylene for 60 min and N_2 for 120 min at ambient temperature, followed by thermal desorption at 250 °C. Note the loss of mass during ambient-temperature purge of C-B.

Figure 2 shows the results of separate TGA tests involving exposure of C-X (2.9 mg, Figure 2a) and C-B (2.9 mg, Figure 2b) to m-xylene vapor. For C-X, exposure to 65 mg/m^3 for 100 min resulted in a mass uptake of 24 µg (8,300 µg/g). The linear uptake over time is consistent with (unrestricted) adsorption well below the W_e value of ~38,000 µg/g at this concentration (see Figure S8†). The TGA sample was then purged with N_2 for 120 min at ambient temperature and there was no evidence of any off-gassing, as expected. Heating to 250 °C resulted in desorption of the m-xylene and recovery of the baseline with only minor drift.

The same test with C-B at 78 mg/m^3 of m-xylene resulted in an uptake of ~15 µg (5,200 µg/g) over a 50-min exposure period, which is also below the estimated W_e value of ~14,000 µg/g at this concentration. In this case, however, the subsequent N_2 purge at ambient temperature resulted in a loss of 2.5 µg (17%) over 120 min from off-gassing. This portended a potential loss of vapor from the µPP during periods of non-exposure. Thermal desorption led to baseline recovery.

µPP desorption/transfer conditions

To establish baseline operating conditions, exposure of the μPP to m-xylene in the test chamber at modest concentrations (~ 44 mg/m^3) over 0.25 hr was followed by desorption at 5 or 10 mL/min at 250 °C for 60 sec. Following the initial desorption/transfer, two additional desorption/transfer steps were run to check for residual vapor. *DE* values for the first desorption/transfer were > 96% in all cases and were consistent among replicate tests (RSD = 4%). Note that the capture and desorption efficiencies of the μPCF were checked by a series of challenges with m-xylene and DEMP at 5 mL/min. No evidence of breakthrough or residual vapor was detected.

For one series of tests a mini-PID was inserted between the μPP and the mini-pump. For transferred masses of 23-25 ng (i.e., 12 mg/m^3 exposure), the desorption profile was asymmetric, but all of the m-xylene was transferred within ~30 sec at 250 °C at both 3 and 5 mL/min. See Figure S10† in Section S6†.

Desorption/transfer tests were then run with DMMP and DEMP, which are less volatile than m-xylene but also more polar. Results for DMMP, for different flow rates and transfer times, showed that for captured masses of 160-200 ng (0.25-hr exposure to 24-30 mg/m^3) the *DE* was 99% at 5 mL/min for a T_{max} of 250 °C for 60 sec (see Table S2†). For DEMP, under the same conditions the *DE* value was only 85%. Increasing T_{max} to 275 °C improved the DE to 94% (see Table S3†). Regardless, the effective sampling rate did not change.

To explore the potential loss of captured vapors during periods of non-exposure, tests were run with o-xylene, DMMP, and DEMP involving an initial exposure followed by either a 4-min or 60-min chamber purge at ambient temperature prior to desorption and transfer. The experimental S_e value was used as the evaluation metric. For o-xylene, consistent with the TGA results for C-B, there was a 6% reduction in S_e between the 4-min and 60-min purge trials. For DMMP there was a 19% reduction, and for DEMP there was no reduction. Results are compiled in Table S4†. Surprisingly, the DMMP had the greatest apparent loss of mass from off-gassing despite its vapor pressure being much lower than that of o-xylene. Clearly, a fraction of the DMMP and to a lesser extent, o-xylene, is only weakly adsorbed on the C-B and can spontaneously desorb at room temperature to a small but significant extent and be lost from the sample.

Sampling rate stability: concentration

The next series of experiments explored the consistency of S_e values for o-xylene over a range of concentrations for a fixed, short exposure period of 0.25 hr. As shown in Figure 3, the experimental S_e value remained within 8% of the starting value over a concentration range of 0.6 to 1,500 mg/m^3, and a corresponding mass uptake range of 6 to 14,000 ng. Remarkably, the *DE* values remained > 96% throughout.

Over the course of the study, other vapors were tested over more modest concentration ranges with no apparent change in S_e values. For example, the S_e value of 0.25 mL/min for DEMP did not change between 1.4 and 87 mg/m^3, and that of DMMP (i.e., 0.44 mL/min) did not change between 3.2 and 49 mg/m^3.

Sampling rate stability: duration

Two series of experiments were run to assess the consistency of S_e over discrete time periods ranging from 0.25 to 24 hr. Results are summarized in Figures 4 and 5 for DEMP and o-xylene, respectively. For exposure to 1.4 mg/m^3 of DEMP (except for 0.25-hr sample at 55 mg/m^3), S_e remained constant up to 4 hr, decreased by 8% for the 12-hr sample, and

decreased by 23% for the 24-hr sample (both relative to the initial 0.25-hr sample). The range of collected (transferred) masses was 25 to 400 ng (i.e., 16-fold), and *DE* values were > 83% in all cases (T_{max} = 250 °C) and did not vary with the uptake mass.

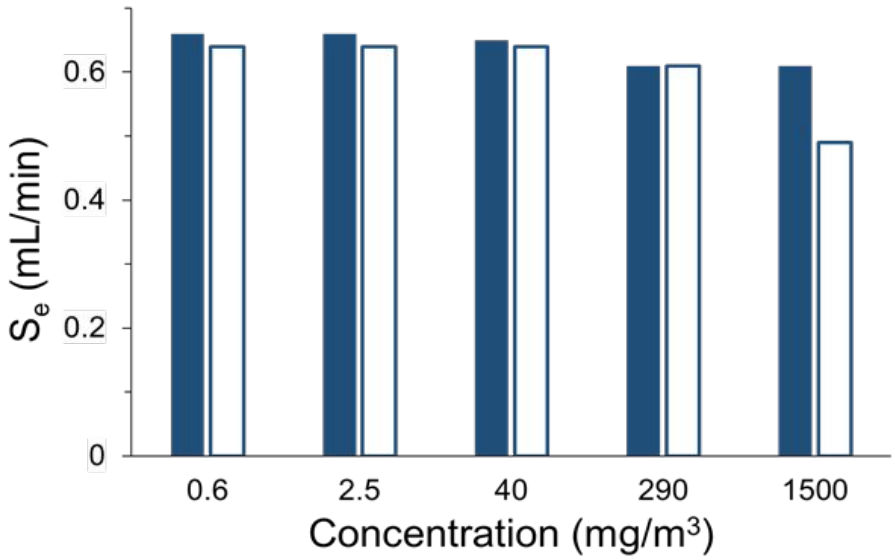

Figure 3 Plot of measured (filled) and modeled (unfilled) S_e values for o-xylene as a function of concentration (0.25-hr samples). The collected mass ranged from 6.1 to 14 µg and DE values were > 96%. There is < 8% reduction in sampling rate over a 2,500-fold concentration range. Agreement between experimental and modeled S_e values is within 3%, except at 1500 mg/m^3 where the modeled underestimates the observed S_e by 19%.

For o-xylene, S_e decreased steadily over time: within the first 4 hr it decreased up to 15% and for the 24-hr sample it decreased by 30% (relative to the initial 0.25-hr sample). Note that the data shown in Figure 5 for the 0.5- and 1-hr samples were collected after the other data were collected and entailed exposures at much higher concentrations (i.e., 124 mg/m^3 in both cases). Despite this, the S_e values were consistent with those collected at the lower average concentration of ~3.5 mg/m^3 used in the other tests. The range of collected masses was from 25 to 4,300 ng (i.e., 172-fold). *DE* values were > 97% in all cases.

These results show that 24-hr sampling is feasible with the µPP with only a small reduction in S_e. The modeling presented in the next section accounts for this reduction.

Modeling of S_e

Table 2 gives the diffusional path length, L_i, and cross section area, A_i, for each formal segment, *i*, of the diffusion path shown in Figure 1b. Note that A_1 in Table 2 assumed apertures with lateral dimensions of 50 × 50 µm. In the fabricated devices, these dimensions were actually 47 ×47 µm, and A_1 is therefore 0.52 mm^2. Detailed descriptions of the segments, and the model derivation and implementation are provided in Section S7†.

Briefly, eq. 1 expresses S_e as a function of the sampling rates, S_1-S_7, in each of the respective segments, S1-S7. The response time, which we define as the time required to establish steady-state conditions at the outer edge of the outer adsorbent bed, is 30 msec for o-xylene, and the largest value among the tested compounds is 78 msec (DIMP) (see Table S4†). Given how rapidly steady-state is established, we refer to this as the "time- zero" value S_e in the next section.

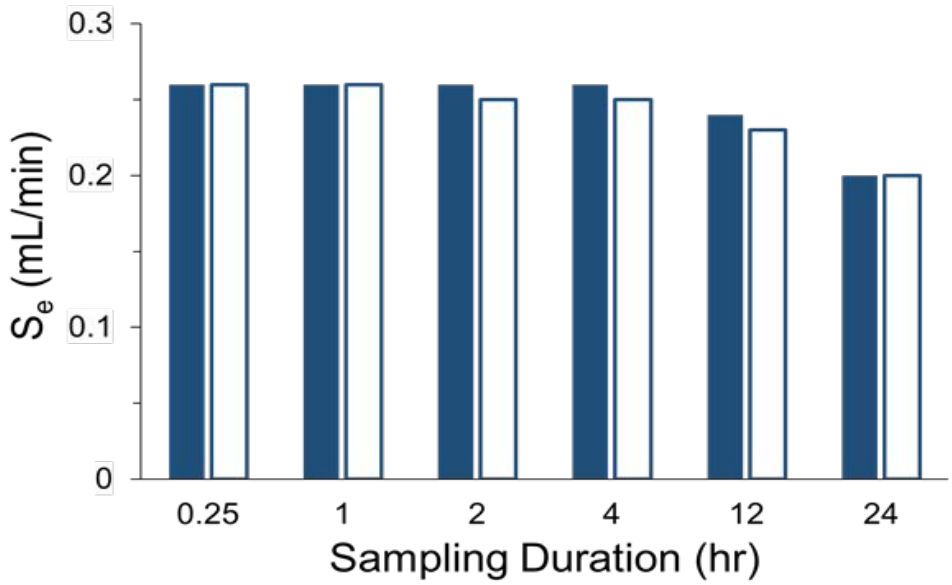

Figure 4 Plot of measured (filled) and modeled (unfilled) S_e values for DEMP as a function of sample duration. The challenge concentration was 1.4 mg/m^3 except for the 0.25-hr test (55 mg/m^3). Note that S_e is constant out to 4 hr, decreases by 8% for the 12-hr sample, and by 23% for the 24-hr sample. The range of transferred masses was from 25 ng to 400 ng, and DE values were > 83% in all cases. Agreement between modeled and experimental values is within 4%.

For the μPP, the sampling rate can change in S5 and S7; as sampling progresses the vapor gradually penetrates S5 first and then (possibly) S7 due to progressive saturation of the adsorbent. Mass transport through the adsorbent bed is impeded by diffusion of the vapor into the pores of adsorbent particles and by adsorption (i.e., retention) of the vapor on the adsorbent surface. The latter can be expressed as a function of W_e, and the former by a $D_{5(7)}$ value that accounts for the expected contribution of Knudsen-like transport within the porous solid.[35]

In the model, changes in the radial length and cross-sectional area in S5 (and S7) over time are expressed in terms of the degree of saturation of the adsorbent bed(s), which is a function of the mass uptake over time, the challenge concentration, and the applicable value of W_e for the compound (and adsorbent) under consideration. Values of D_5 must be determined empirically.

The model was developed and applied first to DEMP and o-xylene using the data in Figures 4 and 5, respectively, concerned with the change in S_e over time. For DEMP, the Fickian D value presented in Table 1 led to an initial modeled value of S_e that was about 20% higher than observed. For the purposes of modeling the *change* in S_e with time, which relies on the value of D_5 determined empirically, we substituted the first modeled S_e value in Figure 4 (i.e., for t = 0.25 hr) with the experimental S_e value, so that the modeled and experimental *changes* were more easily compared.

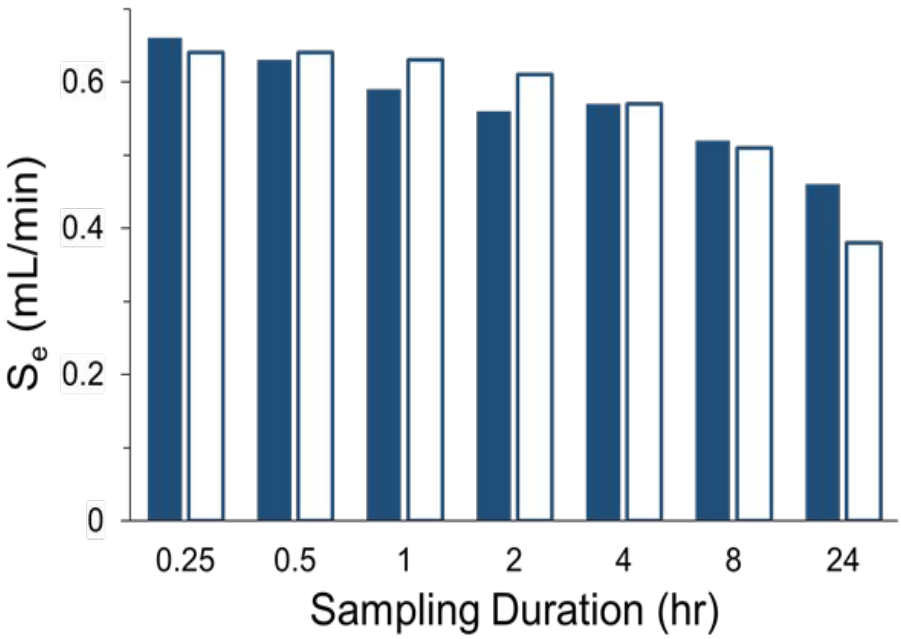

Figure 5. Plot of measured (filled) and modeled (unfilled) S_e values for o-xylene as a function of sample duration. The challenge concentration was 3.5 mg/m^3 except for the 0.5-hr and 1-hr tests (124 mg/m^3). Note that S_e decreases by 21% for the 8-hr sample, and by 30% for the 24-hr sample. The range of transferred masses was from 25 ng to 4,300 ng, and DE values were > 97% in all cases. Agreement between modeled and experimental values is within 8%, except for the 24-hr test where the modeled value is 18% too low.

As shown in Figures 3-5, the modeled and experimental S_e values are generally similar; i.e., within 4% for DEMP and within 8% for o-xylene, with the exception of the 24-hr sample for o-xylene, where the model underestimates S_e by 18%. For both compounds, modeling indicates eventual penetration into the C-X bed. For DEMP at 1.4 mg/m^3, this is expected after 1430 min (i.e., ~24 hr) and for o-xylene at 3.5 mg/m^3 after 820 min (i.e., ~14 hr).

For the 0.25-hr exposures to o-xylene at different concentrations presented in Figure 3, the modeled values are within 3% of the experimental values, except at 1,500 mg/m^3 where the model underestimates S_e by 19%. The latter error may be attributable, in part, to an underestimate in the assumed value of W_e for which there is considerable uncertainty at this

high concentration (see Figure S8†). Notably, even at 1,500 mg/m^3 the model indicates that only 72% of the C-B bed mass would be saturated. Thus, over this very broad range of concentrations, there is no penetration into the C-X bed for o-xylene, and, by inference, for DEMP, over the 0.25 hr time period.

Sampling rates for other compounds

The μPP device was exposed to additional compounds individually for 0.25 hr at modest concentrations of 15 to 200 mg/m^3 to evaluate their S_e values. Results, summarized in Table 1, show that the range of experimental S_e values spans from 0.16 mL/min (DMSO) to 0.78 mL/min (NBZ); a 4.9-fold range. The reported values are representative, and for all but one compound (i.e., NMP), the S_e values were quite reproducible among separate tests (e.g., RSDs were ≤ 4% for triplicate runs of several other compounds). *DE* values for most compounds were ≥ 90% (exceptions: DEMP, 80-82%; NMP, decomposition). *DE* values were generally highly reproducible.

The modeled S_e values listed in Table 1 were calculated assuming no penetration into the C-B bed (i.e., at $t = 0$ hr). As a check, those compounds for which estimates W_e on C-B could be made were also modeled at t = 0.25 hr and the S_e values differed by < 2% from those at t = 0 hr. For n-butanol, no significant adsorption on C-B was expected,[45] so the modeled S_e value assumes that steady state was established at the outer edge of the C-X bed (i.e., segment S7). The same assumption was made for the modeled S_e value of DMF in Table 1.

Comparing modeled to experimental S_e values, the results were mixed. For the first nine compounds listed in Table 1 (i.e., m-xylene to NBZ), the ratios of modeled-to-experimental S_e values ranged from 0.90 to 1.1, indicating excellent agreement. For the remaining six compounds, the modeled values overestimated the experimental values by > 15%. For DEMP and DIMP, we believe that the (Fickian) *D* values may be in error (see Section S8 of the ESI). For NMP and DMSO there is literature to suggest thermal decomposition at 260 and 190 °C, respectively.[46,47] Interestingly, however, the DMSO results were quite reproducible among four replicate trials (RSD < 6%). The GC traces from the tests with these compounds gave no evidence of decomposition products. Thus, DMSO can be sampled and transferred reliably, but this is not the case for NMP.

The modeled S_e values for n-butanol and DMF also overestimated the experimental values by considerable margins. The most likely explanation is that both of these compounds penetrate the C-X bed even over the short exposure period tested. For n-butanol, this is supported by the study cited above (ref. 45), which showed a relatively small breakthrough mass with a C-X packed adsorbent tube, and a rather low estimate of W_e derived from that data. Although the modeled "time zero" S_e value (Table 1) of n-butanol is 0.49 mL/min, it is predicted to saturate the C-X bed within 10 min of exposure at the high challenge concentration of 198 mg/m^3 used in the test. Assuming no further vapor uptake over the ensuing 5 min, and no loss due to off-gassing, the modeled S_e value would be 0.28 mL/min, which is within 10% of the experimental S_e of 0.31 mL/min reported in Table 1. Although the DMF capacity of C-X could not be found in the literature, we speculate that a similar phenomenon could explain its low experimental S_e value.

The last column in Table 1 presents the mass of each compound that would be collected from a 0.5-hr sample at a concentration of 0.05 mg/m^3, assuming that the experimental S_e value shown would apply to this low concentration. Recall, that we designed the μPP to

collect ≥ 0.5 ng under this scenario. As shown, for 11 of the 15 compounds, this criterion is met or exceeded. Others would require just an additional 2 to 29 min to collect the stipulated minimum mass (exception: NMP, per above).

Mixtures

Tests with mixtures of vapors were performed to explore whether competitive adsorption among different compounds might lead to displacement of one compound by another. o-Xylene and DEMP, which are both captured in the C-B bed and have similar estimated W_e values, but differ significantly in volatility and polarity, were chosen for these experiments. Observed S_e values were used as an indirect measure of any loss of vapor. Individual exposures were 0.25 hr and mixture exposures were 0.5 hr in duration. Results are summarized in Figs. 6 and 7 (and Tables S6 and S7†).

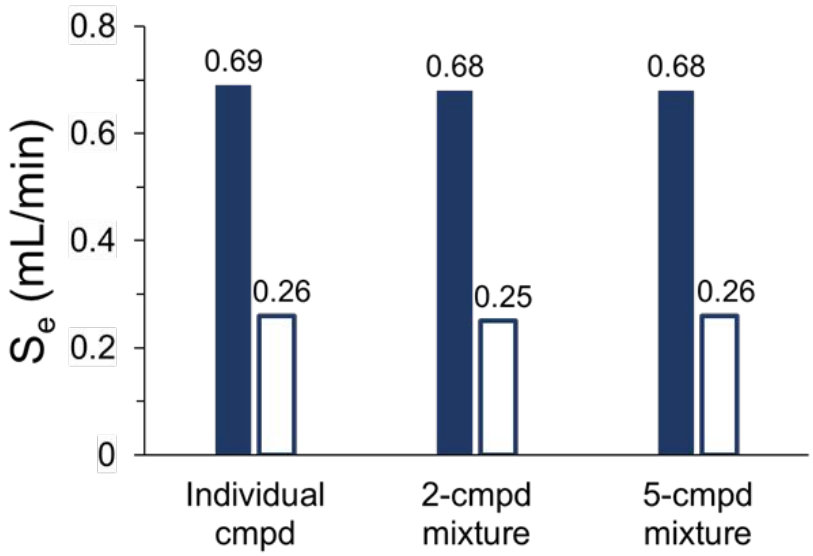

Figure 6 Se values of o-xylene (filled) and DEMP (unfilled) exposed for 0.5 hr individually, as a binary mixture (see text for concentrations), and as a mixture with DMSO (140 mg/m^3), DIMP (19 mg/m^3), and NMP (8 mg/m^3). For the latter, the o-xylene and DEMP concentrations were 110 and 14 mg/m^3, respectively. Analysis was by GC-FID.

Individual exposures to o-xylene and DEMP (45 mg/m^3 each) resulted in uptake masses of 440 and 190 ng, respectively, and yielded S_e values of 0.69 and 0.26 mL/min, respectively, in close agreement with the values in Table 1. Exposure to a binary mixture of o-xylene (360 mg/m^3) and DEMP (87 mg/m^3) resulted in uptake masses of 7,500 and 660 ng, respectively, with virtually no changes in the S_e values observed in the individual exposures. A follow-up test with three additional compounds added to a mixture of these two compounds, also had no effect on the S_e values obtained for o-xylene and DEMP. Finally, exposure to a mixture of eight compounds yielded the S_e values shown in the chromatogram presented in Figure 7, all eight of which agree closely with the values in

Table 1 (and Figure 6). This confirms that the μPP has sufficient capacity to avoid losses due to displacement among competing vapors.

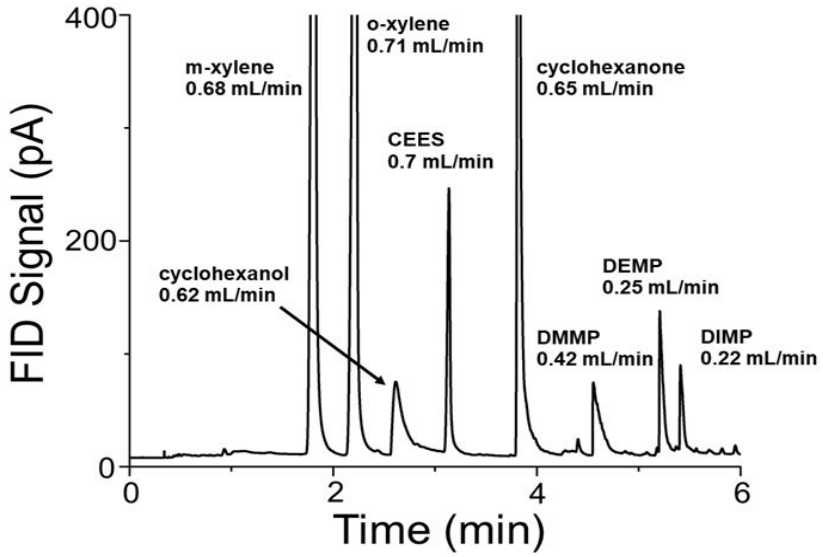

Figure 7 GC-FID chromatogram of an 8-vapor mixture passively sampled with the μPP, transferred to the μPCF, and injected. Separation used a 15 m RTX-200 column at 30 °C for 2.5 min, followed by 30 °C/min to 125 °C, then hold. The concentrations of the 8 vapors ranged from 2 mg/m^3 (cyclohexanol) to 12 mg/m^3 (cyclohexanone) and injected masses from 37 to 250 ng. DE values were > 95% except for DEMP and DIMP (80 and 82%, respectively).

Conclusions

We conclude that the μPP has numerous positive attributes that favor its use as part of the micro Collector-Injector (μCOIN) we are developing for μGC analysis of S/VOC mixtures. Its ability to sample S/VOCs at predictable rates with zero expended energy is particularly enabling when sampling for longer time periods where pumping would dominate the energy consumption for the μGC system. The modeled and experimental sampling rate values for the 15 (predominantly polar) compounds tested agree sufficiently well to verify the design strategy applied to the μPP and the modeling assumptions (exceptions noted and explained). Substantial advantages of the μPP over the previous passive micro-preconcentrator developed in our group[23] accrue from the complete redesign and include the radial topology, higher capacity, larger analyte range, no apparent competitive displacement by mixture components, lower desorption flow rate, longer sampling duration, and more robust fabrication process.

Measured (diffusional) μPP sampling rates are independent of concentration and are sufficiently high to collect ~ng quantities in sampling periods of 30-60 min for most

compounds at concentrations ≥ 50 μg/m^3. Yet, sampling rates stay sufficiently constant to allow quantitative measurements at much higher concentrations or over sampling periods as long as 24 hr. These features are adequate to serve the needs of numerous practical applications. The use of dual adsorbents enabled efficient sampling, thermal desorption, and transfer of most of the (predominantly polar) test compounds. Partial off-gassing during extended post-exposure time periods was observed with o-xylene and DMMP due to weak adsorption on the C-B. The fractional loss was significant for DMMP, and indicates that desorption/transfer cycle times would need to be constrained.

The semi-empirical model developed to describe the changes in the sampling rate with time and concentration accounts for the physicochemical processes governing the dynamics of vapor transport and uptake within the μPP. Implementation requires the Fickian D value, the vapor concentration, and the W_e value for one or both adsorbents at the exposure concentration. In addition, the reduced D value applicable to transport through the porous adsorbent bed(s) is needed. Notably, although Fickian D values of many compounds in air can be found in the literature or calculated by the classical Fuller method, D values for organophosphonates are virtually absent from the literature we searched and cannot be calculated by known models.

In the next-generation μPP design, we plan to add a third adsorbent bed packed with a higher-surface-area adsorbent to enable the capture of more volatile and polar compounds. A companion publication is being prepared describing the μPHI that has been developed as part of the larger project concerned with the ultimate μCOIN. Integrating the μPP with the μPHI in a monolithic μCOIN device is also underway.

Conflicts of interest

The authors declare no conflicts.

Acknowledgements

The authors would like to thank the following individuals: Dr. Lexuan Zhong for early help with GC calibrations; Fernando Almazán Román for early TGA testing; Junqi Wang for training and problem solving; Jon Bryant-Genevier for training on μPCF operation; Sanketh Buggaveeti, Rob Nidetz, and Katsuo Kurabayashi for designing the μPCF heater and fabricating μPCF devices; Will Collin for GC training; Brendan Casey for wire-bonding; Tom Daunais for assistance with fabrication; Bjoern Brixius for performing selected GC calibrations; and Clementine Kornder for administrative coordination. Devices described in this paper were fabricated in the Lurie Nanofabrication Facility at the University of Michigan. This research was supported by Contract # 2017-17012600004 from the Office of the Director of National Intelligence (ODNI), Intelligence Advanced Research Projects Activity (IARPA). The views and conclusions contained herein are those of the authors and should not be interpreted as representing the official policies, either expressed or implied, of ODNI, IARPA, or the U.S. Gov't. Additional (seed) funding was provided by Grant # T42 OH008455, from the Centers for Disease Control and Prevention (CDCP). The contents herein are solely the responsibility of the authors and do not necessarily represent the official views of the CDCP.

References

1 S. Zampolli, I. Elmi, F. Mancarella, P. Betti, E. Dalcanale, G. Cardinali and M. Severi, *Sens. Actuators, B*, 2009, **141**, 322-328.

2 S. K. Kim, H. Chang and E. T. Zellers, *Anal. Chem.*, 2011, **83**, 7198-7206.

3 R. Manginell, J. Bauer, M. Moorman, L. Sanchez, J. Anderson, J. Whiting, D. Porter, D. Copic and K. Achyuthan, *Sensors*, 2011, **11**, 6517-6532.

4 W. R. Collin, G. Serrano, L. K. Wright, H. Chang, N. Nuñovero and E. T. Zellers, *Anal. Chem.*, 2013, **86**, 655-663.

5 A. Garg, M. Akbar, E. Vejerano, S. Narayanan, L. Nazhandali, L. C. Marr and M. Agah, *Sens. Actuators, B*, 2015, **212**, 145-154.

6 M. Akbar, M. Restaino and M. Agah, *Microsyst. Nanoeng.*, 2015, **1**, 15039.

7 W. R. Collin, A. Bondy, D. Paul, K. Kurabayashi and E. T. Zellers, *Anal. Chem.*, 2015, **87**, 1630-1637.

8 Y. Qin and Y. B. Gianchandani, *Microsyst. Nanoeng.*, 2016, **2**, 15049.

9 M. Zhou, J. Lee, H. Zhu, R. Nidetz, K. Kurabayashi and X. Fan, *RSC Adv.*, 2016, **6**, 49416-49424.

10 J. Wang, J. Bryant-Genevier, N. Nuñovero, C. Zhang, B. Kraay, C. Zhan, K. Scholten, R. Nidetz, S. Buggaveeti and E. T. Zellers, *Microsyst. Nanoeng.*, 2018, **4**, 17101.

11 J. Wang, N. Nuñovero, R. Nidetz, S. J. Peterson, B. M. Brookover, W. H. Steinecker and E. T. Zellers, *Anal. Chem.*, 2019, **91**, 4747-4754.

12 J. J. Whiting, E. Myers, R. P. Manginell, M. W. Moorman, J. Anderson, C. S. Fix, C. Washburn, A. Staton, D. Porter and D. Graf, *Lab Chip*, 2019, **19**, 1633-1643.

13 APIX ANALYTICS, https://www.apixanalytics.com/, (accessed October 2019).

14 Zebra ANALYTIX, https://zebraanalytix.com/technology/, (accessed October 2019).

15 TCM Global, https://www.tcmglobalinc.com/, (accessed October 2019).

16 Omniscent, https://omniscent.com/, (accessed October 2019).

17 W.-C. Tian, H. K. Chan, C.-J. Lu, S. W. Pang and E. T. Zellers, *J. Microelectromech. Syst.*, 2005, **14**, 498-507.

18 E. H. M. Camara, P. Breuil, D. Briand, N. F. de Rooij and C. Pijolat, *Anal. Chim. Acta*, 2011, **688**, 175-182.

19 T. Sukaew and E. T. Zellers, *Sens. Actuators, B*, 2013, **183**, 163-171.

20 J. Bryant-Genevier and E. T. Zellers, *J. Chromatogr. A*, 2015, **1422**, 299-309.

21 R. P. Manginell, D. R. Adkins, M. W. Moorman, R. Hadizadeh, D. Copic, D. A. Porter, J. M. Anderson, V. M. Hietala, J. R. Bryan and D. R. Wheeler, *J. Microelectromech. Syst.*, 2008, **17**, 1396-1407.

22 R. P. Manginell, S. Radhakrishnan, M. Shariati, A. L. Robinson, J. A. Ellison and R. J. Simonson, *IEEE Sens. J.*, 2007, **7**, 1032-1041.

23 J. H. Seo, S. K. Kim, E. T. Zellers and K. Kurabayashi, *Lab Chip*, 2012, **12**, 717-724.

24 J. H. Seo, J. Liu, X. Fan and K. Kurabayashi, *Lab Chip*, 2013, **13**, 851-859

25 M. Akbar, N. Nuñovero, R. Hower, C. Zhan, J. Potkay and E. Zellers, *2018 Solid-State Sensors, Actuators & Microsystems Workshop*, Hilton Head Island, USA, 2018.

26 C. Zhan, M. Akbar, R. Hower, J. Wang, N. Nuñovero, J. A. Potkay and E. T. Zellers, *the 20th International Conference on Solid-State Sensors*, Actuators and Microsystems, Berlin, Germany, 2019.

27 IARPA, Molecular Analyzer for Efficient Gas-phase Low-power INterrogation (MAEGLIN). https://www.iarpa.gov/index.php/research-programs/maeglin (accessed June, 2020).

28 E. Palmes and A. F. Gunnison, *Am. Ind. Hyg. Assoc. J.*, 1973, **34**, 78-81.

29 E. V. Kring and W. J. Lautenberger, US Pat., 4,235,097, 1980.

30 J. L. Perkins, Modern Industrial Hygiene: Recognition and Evaluation of Chemical Agents, ACGIH, Cincinnati, 2008.

31 G. O. Wood and E. S. Moyer, *Am. Ind. Hyg. Assoc. J.*, 1991, **52**, 235-242.

32 F. Rouquerol, J. Rouquerol, K. S. W. Sing, P. Llewellyn and G. Maurin, *Adsorption by powders and porous solids: principles, methodology and applications*, Academic press, New York, 2013.

33 A. Wheeler and A. Robell, *J. Catal.*, 1969, **13**, 299-305.

34 U.S. National Library of Medicine, https://toxnet.nlm.nih.gov/cgi-bin/sis/htmlgen?HSDB, (accessed October 2019).

35 M. Tang, M. Shiraiwa, U. Pöschl, R. Cox and M. Kalberer, *Atmos. Chem. Phys.*, 2015, **15**, 5585-5598.

36 J. T. Hunter and N. L. Abbott, *Sens. Actuators, B*, 2013, **183**, 71-80.

37 D. A. Trubitsyn and A. V. Vorontsov, *J. Phys. Chem. B*, 2005, **109**, 21884-21892.

38 VEGA ZZ Manual, https://nova.disfarm.unimi.it/manual/pages/gl_index.htm, (accessed October 2019).

39 G. Serrano, T. Sukaew and E. T. Zellers, *J. Chromatogr. A*, 2013, **1279**, 76-85.

40 C. J. Lu and E. T. Zellers, *Analyst*, 2002, **127**, 1061-1068.

41 J. Brown and R. Shirey, Supelco Technical Report -- A Tool for Selecting an Adsorbent for Thermal Desorption Applications, https://www.sigmaaldrich.com/content/dam/sigma-aldrich/docs/Supelco/General_Information/t402025.pdf, (accessed October 2019).

42 H. Zhu, R. Nidetz, M. Zhou, J. Lee, S. Buggaveeti, K. Kurabayashi and X. Fan, *Lab Chip*, 2015, **15**, 3021-3029.

43 C. C. Mulligan, N. Talaty and R. G. Cooks, ChemComm, 2006, 1709-1711.

44 G. O. Nelson, *Gas mixtures: preparation and control*, CRC Press, Boca Raton, 1992.

45 J. Wang, J. Ma, and E. T. Zellers, *J. Chrom. A* 2020, **1609**, 460486

46 M. Bollyn, *Organic Process Research & Development*, 2006, **10**, 1299-1312.

47 A. M. White and B. M. Sankey, US Patent, 4,168,226, 1979.

TOC entry

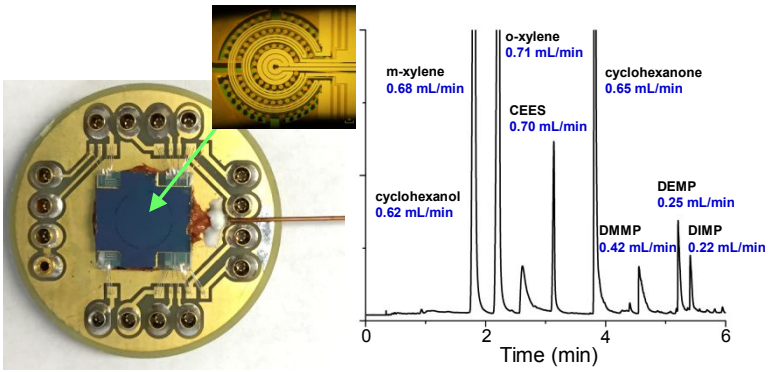

We demonstrate “zero-power” sampling at known rates for up to 24 hr, high capacity, and high desorption (transfer) efficiency for downstream separation and detection